Title
Characterization of a HPHT boron ion-implanted diamond X-ray mirror following high vacuum annealing

Authors
Margraf-O'Neal, RA
Ynsa, MD
Krzywinski, J
et al.

Publication Date
2024-06-01

DOI
10.1016/j.diamond.2024.111212

Graphical Abstract

Characterization of a HPHT Boron Ion-Implanted Diamond x-ray Mirror following High Vacuum Annealing

R. A. Margraf,M. D. Ynsa,J. Krzywinski,A. Halavanau,M. L. Ng,J. P. MacArthur,F. Ke,Y. Zhong,S.-K. Mo,P. Pradhan,R. Robles,A. Robert,T. Sato,D. Zhu,G. Marcus

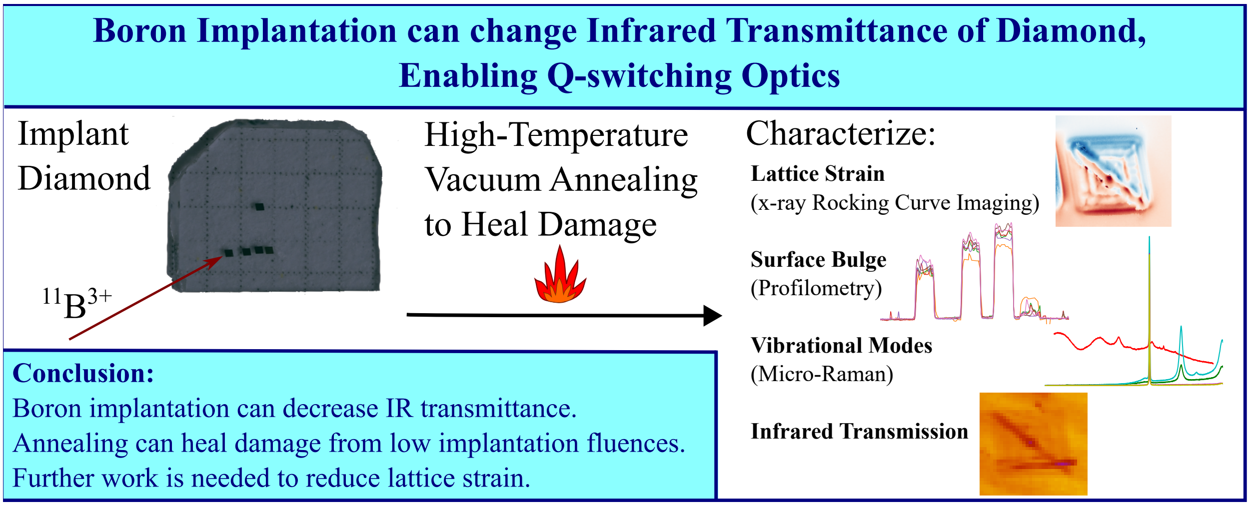

Highlights

Characterization of a HPHT Boron Ion-Implanted Diamond x-ray Mirror following High Vacuum Annealing

R. A. Margraf,M. D. Ynsa,J. Krzywinski,A. Halavanau,M. L. Ng,J. P. MacArthur,F. Ke,Y. Zhong,S.-K. Mo,P. Pradhan,R. Robles,A. Robert,T. Sato,D. Zhu,G. Marcus

- Boron ion implantation can increase the infrared absorption of diamond
- High temperature annealing can repair a diamond lattice below a damage threshold
- x-ray rocking-curve imaging and micro-Raman spectroscopy can assess lattice quality
- Surface profilometry can also provide insight into diamond lattice repair

Characterization of a HPHT Boron Ion-Implanted Diamond x-ray Mirror following High Vacuum Annealing

R. A. Margraf[a,b], M. D. Ynsa[c], J. Krzywinski[a], A. Halavanau[a], M. L. Ng[a], J. P. MacArthur[a], F. Ke[b], Y. Zhong[b], S.-K. Mo[d], P. Pradhan[e], R. Robles[a], A. Robert[b,f], T. Sato[a], D. Zhu[a] and G. Marcus[a]

[a] *SLAC National Accelerator Laboratory, 2575 Sand Hill Rd, Menlo Park, 94025, CA, USA*
[b] *Stanford University, 450 Jane Stanford Way, Stanford, 94305, CA, USA*
[c] *Center for Micro Analysis of Materials, Autonomous University of Madrid, Campus de Cantoblanco, C/ Faraday 3, Madrid, 28049, Spain*
[d] *Lawrence Berkeley National Laboratory, 1 Cyclotron Road, Berkeley, 94720, CA, USA*
[e] *Argonne National Laboratory, 9700 S. Cass Avenue, Lemont, 60439, IL, USA*
[f] *MAX IV Laboratory, Fotongatan 2 , Lund, 224 84, Sweden*

ARTICLE INFO

Keywords:
diamond crystal
synthetic diamond
high pressure high temperature (HTHP)
implantation
optical properties characterization
surface characterization
vibrational properties characterization
optical properties
strain
vibrational properties

ABSTRACT

High energy boron ion implantation of diamond promises to lead to advances in x-ray optics by enabling the ability to tune parameters of the diamond lattice. For example, a boron-doped diamond lattice can have increased infrared absorption compared to pure diamond, enabling Q-switchable optics [1]. For these optics to be useful as Bragg-reflecting mirrors, ion implantation must be performed while maintaining a strain-free perfect diamond lattice. Here, we document a series of high energy boron ion implantations in diamond, and a series of high-temperature vacuum annealings used to heal the diamond lattice. We characterize the healing of the diamond lattice using x-ray rocking curve imaging, surface profilometry, and micro-Raman spectroscopy, and also report the infrared transmission.

1. Introduction

Synthetic diamond crystals, grown with chemical vapor deposition (CVD) or in high-pressure high-temperature (HPHT) chambers have become increasingly important in the semiconductor industry, as well as in x-ray optics. Diamond has several exceptional properties, including the widest electronic band gap, highest breakdown voltage and carrier mobility among known semiconductors [2]. Additionally, due to its low Z number and lattice constant, diamond is a near-perfect reflector of hard x-rays when used in Bragg-reflecting optics. A key obstacle to wide synthetic diamond applications remains to be doping. Whether dopants are introduced in the diamond via epitaxy or ion implantation, the process presents significant challenges due to diamond's tight lattice. For example, when diamond is doped with boron, it is common for carbon atoms to form B-C bonds which naturally distort the crystal lattice. This distortion is highly detrimental to the use of doped diamonds as Bragg-reflecting x-ray optics, as many applications utilize the narrow diamond Darwin width in hard x-ray range (e.g. 7.6 µrad for diamond 400 at 9.831 keV [3]).

However, recently it was proposed that successful diamond doping with high energy boron implantation can preserve the original lattice structure, and open a new avenue in Q-switched x-rays optics [1]. In this case, only one dopant (Boron) needs to be introduced at a specific depth and ion concentration. The boron doped layer, due to the difference in IR absorption properties, may then work as a Q-switching x-ray reflector, allowing for controllable expansion of the diamond lattice on demand. Such control would allow the Bragg reflectivity at a specific angle to be quickly turned on and off at the 10s of ns scale.

In this paper we present a comprehensive characterization of a boron ion implanted diamond sample, focusing on the potential applications of this sample in x-ray optics experiments. In this paper, we first discuss the boron

rmargraf@stanford.edu (R.A. Margraf)
ORCID(s): 0000-0003-3063-1818 (R.A. Margraf); 0000-0002-7624-0794 (M.D. Ynsa); 0000-0002-5879-9578 (A. Halavanau); 0000-0002-1906-9636 (F. Ke); 0000-0003-4242-2503 (Y. Zhong); 0000-0003-0711-8514 (S.-K. Mo); 0000-0003-4003-8794 (P. Pradhan); 0000-0002-7152-4675 (R. Robles); 0000-0002-6371-4196 (A. Robert); 0000-0002-8308-0274 (G. Marcus)

implantation and sample annealing procedures. Afterwards, we report on characterization of the lattice constant, surface flatness, Raman spectroscopy and IR transmittance. Finally, we provide a summary of our findings.

2. Sample Preparation

2.1. Doping recipe procedure

An HPHT diamond sample (6 x 5 x 0.4 mm) was procured from the Element-6 company as described in [1], then implanted as described in [4] with 9 MeV boron ions using the microbeam line at the Center for Micro Analysis of Materials (CMAM) at the Autonomous University of Madrid. 200 x 200 μm areas were implanted with fluences of 5×10^{15}, 1×10^{16},1.5×10^{16} 2×10^{16} and 2.5×10^{16} ions/cm^2 by scanning a focused beam of boron ions in a spiral rastering pattern.

2.2. Annealing procedure

Following implantation, five high-temperature in-vacuum annealings at 900, 950,1150, 1300, and 1450 °C were performed to attempt healing the implantation damage. 900 and 950 °C annealings were performed in a UHV chamber heated by a filament under 2.7×10^{-8} mbar or better vacuum. The filament was heated to the target temperature, then annealed for 1 hr. The 1150, 1300, and 1450 °C annealings were performed in a Red Devil G vacuum furnace manufactured by R. D. Webb Company Inc under 1×10^{-4} mbar or better vacuum, similar to the used in Ref. [5]. The furnace was ramped up at 2 °C/min, annealed for 3 hr, then ramped down at 3 °C/min to 700 °C and cooled.

During this process, we noticed a color change in the least doped, 5×10^{15} ions/cm^2, region, as shown in Fig. B.1, which lightened following the initial 900 °C annealing. We also observed some graphitization, but not noticeably on our regions of interest.

3. Crystal Characterization Results

We performed several measurements to characterize healing in the boron-implanted regions. Rocking curve imaging (RCI) was used to evaluate strain in the crystal lattice, and evaluate the uniformity of rocking curve center across the crystal. Surface profilometry was used to evaluate the healing of the surface bulge created by boron implantation by measuring the surface height of the crystal. Mico-Raman spectroscopy was used to probe the quality of the diamond lattice, where pure diamond should show a strong peak at 1332 cm^{-1}. Finally, we performed IR transmittance measurements to show that boron-doping can increase the IR absorption of diamond, as desired for Q-switching.

3.1. Lattice constant verification with x-ray rocking curve imaging

To assess x-ray reflectivity in the Boron-doped regions, we performed RCI by reflecting off diamond 400 lattice planes. For use as a Bragg-reflecting optic, we expect the diamond RCI to be uniform to better than the rocking curve width (∼10 μrad) over the reflection area. The pre-implantation RCI was performed at BL29XU of SPring-8 at RIKEN with 9.831 keV x-rays. The pre-annealing RCI was performed at the Advanced Photon Source at Argonne National Laboratory with 10 keV x-rays. All annealed RCI were performed at beamline 10-2 of the Stanford Synchrotron Radiation Light Source at SLAC National Accelerator Laboratory with 9.831 keV x-rays [6]. Images were collected as the crystal was rotated, and a Gaussian fit was performed to find rocking curve center and FWHM.

In Fig. 1, annealing decreased the overall deviation in the rocking curve center. It also decreased deviation of the rocking curve center in the implanted regions, particularly in the least doped, 5×10^{15} ions/cm^2 region. However, despite significant healing of the lattice, even in the lowest boron-doped region there are still 10 μrad deviations in the rocking curve center. Since the width of the Bragg rocking curve is also approximately 10 μrad, such deviations are detrimental for use of this sample as a Bragg-reflecting x-ray mirror. We note that for the two pre-annealing datasets, the crystal was rocked left/right, versus up/down in the annealed datasets, explaining some differences in RCI structure.

Fig. 2 shows example single-pixel rocking curves from the 1150 °C annealing dataset. The rocking curves in the boron-doped regions are much broader, and have lower overall reflectivity than the un-doped regions.

3.2. Surface profilometry

We performed a topography measurement on the implanted regions using a Zygo NewView, a 3d white light interferometer. For measuring the entire surface, stitching measurement was performed using a 2.75x objective.

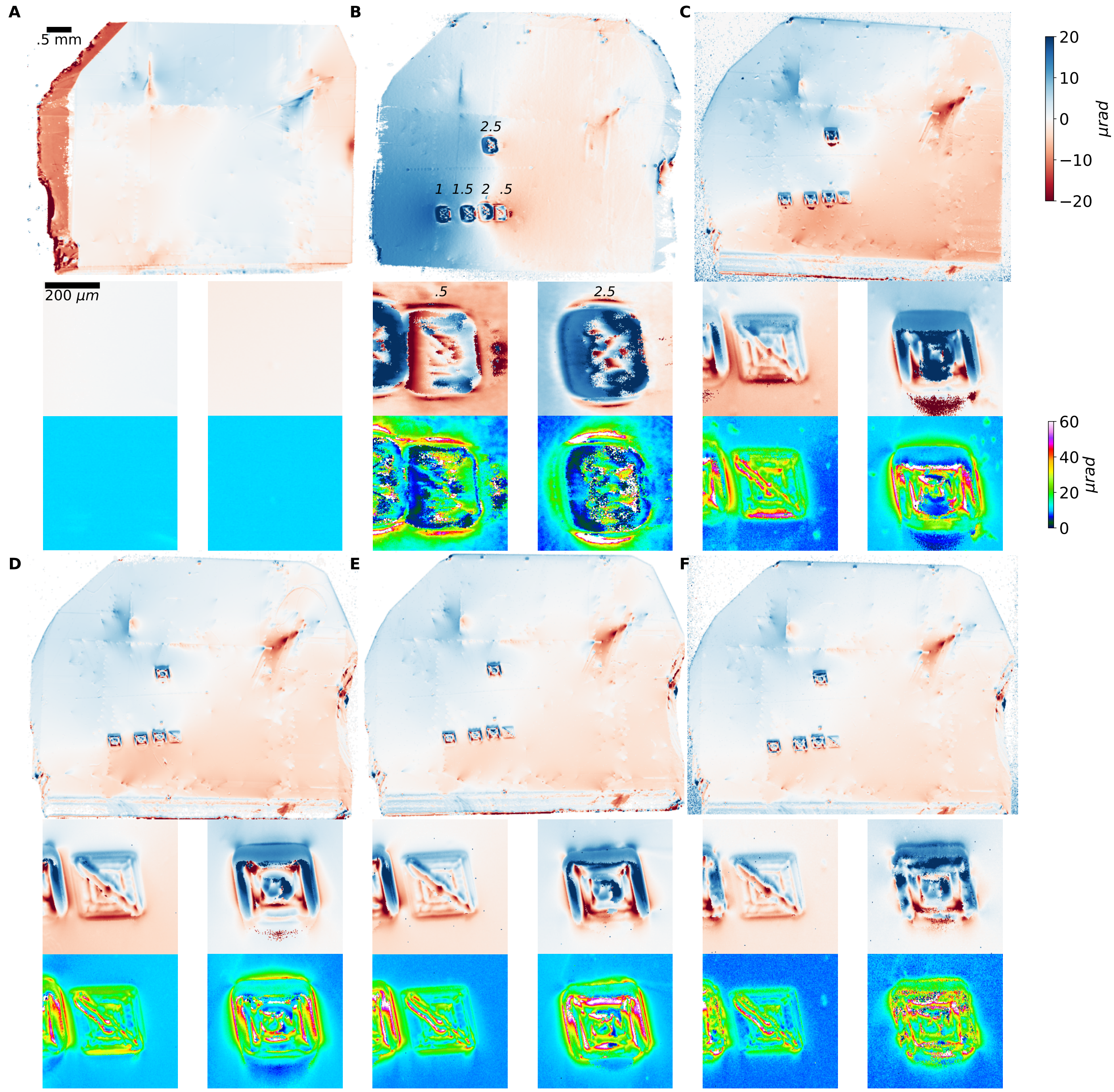

Figure 1: RCI Imaging. A) pre-doping, B) pre-annealing, C) post 950 °C annealing, D) post 1150 °C annealing, E) post 1300 °C annealing, and F) post 1450 °C annealing. Each case shows the rocking-curve center as determined by a Gaussian fit (red-blue colorscale) and the rocking-curve full-width half-maximum (rainbow colorscale). Overlaid numbers give the fluences of the boron implanted regions in units of $1 \times 10^{16}\,\mathrm{ions/cm^2}$. The lower images show close-ups of the boron-doped regions, $5 \times 10^{15}\,\mathrm{ions/cm^2}$ (left) and $2.5 \times 10^{16}\,\mathrm{ions/cm^2}$ (right).

As shown in Fig. 3, pre-annealing, the boron-implanted regions had a surface bulge of 50-150 nm. Each annealing reduced the surface height in the lowest doped, $5{\times}10^{15}$ ions/cm^2 region, with the largest effect occurring after the initial 900 °C annealing. However, at higher fluences, annealing actually increased the height of the boron-doped regions. This suggests annealing promoted rearrangement of the diamond crystal lattice in the boron-implanted regions, but the more highly doped regions could not repair the damage to the lattice from annealing.

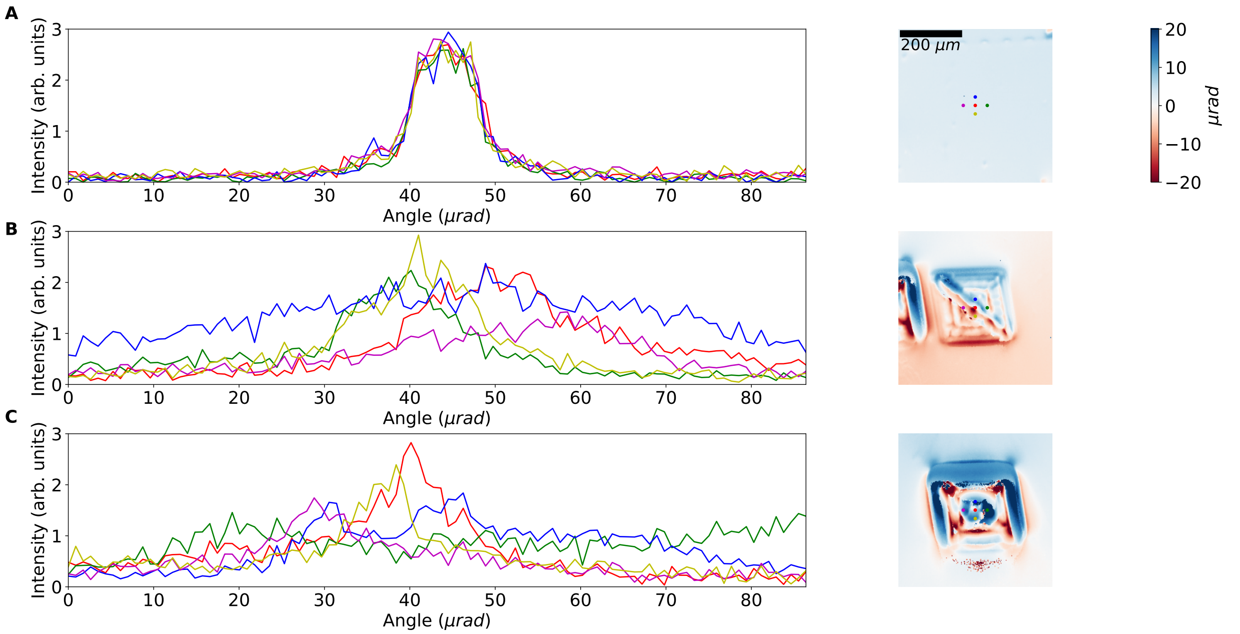

Figure 2: Single pixel rocking curve images from the post $1150\,^{\circ}\mathrm{C}$ annealing dataset. A) Undoped diamond, B) $5 \times 10^{15}\,\mathrm{ions/cm^2}$, C) $2.5 \times 10^{16}\,\mathrm{ions/cm^2}$. The inset images show the locations (indicated by colored dots) within the image where each single-pixel rocking curve was obtained from.

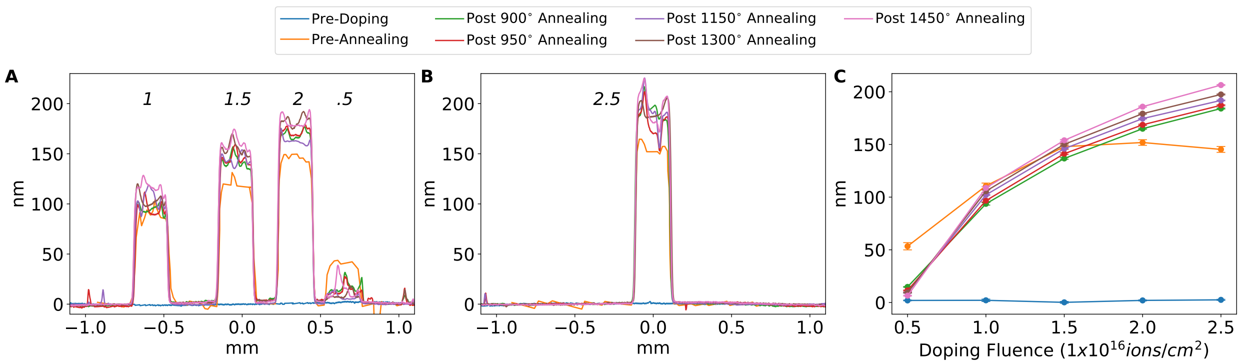

Figure 3: White light surface topography. A-B) Line scans where a quartic background term has been removed. C) Average surface height above surrounding region. Overlaid numbers give the fluences of the boron implanted regions in units of $1 \times 10^{16}\,\mathrm{ions/cm^2}$. Error bars give the standard error of the mean plus systematic errors.

3.3. Micro-Raman Spectroscopy

To assess healing of boron-implanted regions, we performed micro-Raman spectroscopy. A Renishaw inVia Raman Microscope with a 514 nm laser and a Leica 20x/.40 N Plan Epi objective was used on a ~1 - 4 µm area spot.

Pure diamond has a sharp peak in the micro-Raman specta at $1332\,\mathrm{cm^{-1}}$, as shown in Fig. 4. After implantation, the $1332\,\mathrm{cm^{-1}}$ peak decreased for all implanted regions. After $1150\,^{\circ}\mathrm{C}$ and higher annealings, the $1332\,\mathrm{cm^{-1}}$ peak for the lowest boron-doped region recovered to 83 % of the height of the diamond reference peak, as shown in Fig. 4G. However, the more highly boron-doped regions retained a much smaller $1332\,\mathrm{cm^{-1}}$ peak. This suggests annealing at $1150\,^{\circ}\mathrm{C}$ or higher may somewhat heal the crystal lattice of a region doped with boron at a $5\times10^{15}\,\mathrm{ions/cm^2}$ fluence, but higher fluences do not heal. Annealing also changes the micro-Raman background, consistent with earlier studies [7].

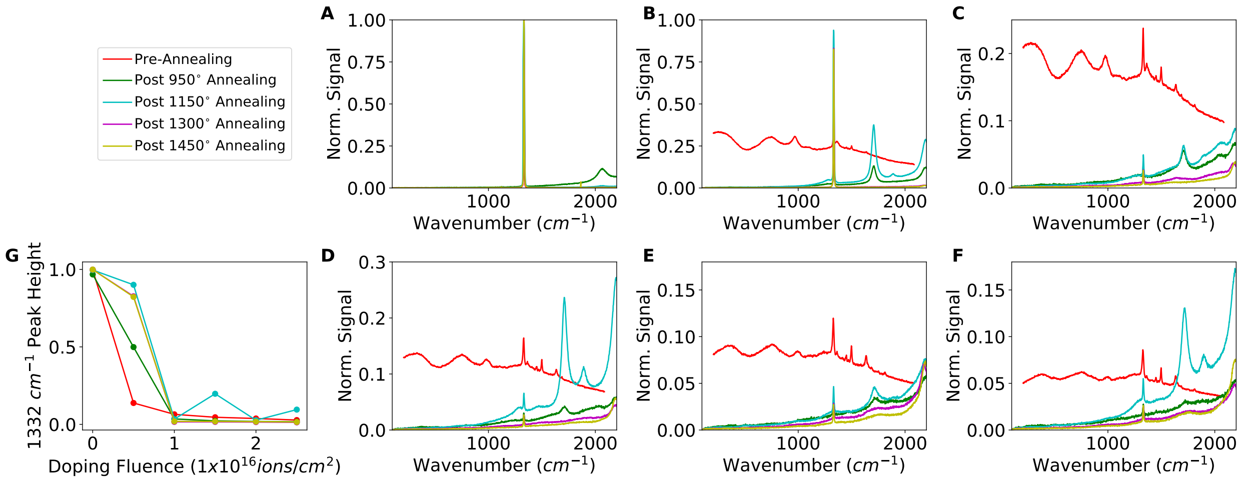

Figure 4: Micro-Raman Spectroscopy for A) pre-annealing, B) post 950 °C annealing, C) post 1150 °C annealing, D) post 1300 °C annealing, and E) post 1450 °C annealing. Each case has been normalized to the height of the 1332 cm^{-1} peak in an un-doped region. G) Plot of the height of the 1332 cm^{-1} peak above background, normalized to the height of the 1332 cm^{-1} peak in an un-doped region.

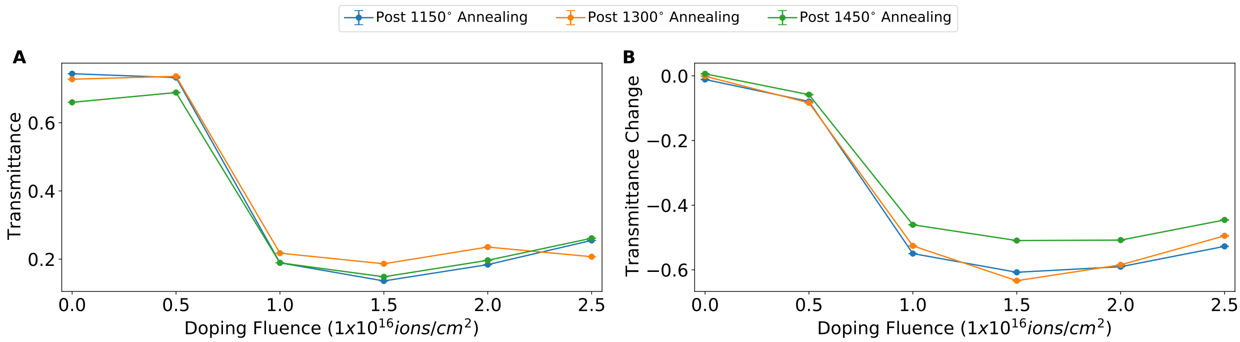

Figure 5: IR transmittance, post 1450 °C annealing. B) IR transmittance by region. C) Transmission of regions versus a region of un-doped diamond directly outside it. Error bars are standard error of the mean.

3.4. IR Transmittance

To show implantation increases IR absorption, we measured IR transmittance, as shown in Fig. 5. A Thorlabs CPS780S laser diode beam was expanded, collimated and transmitted through our sample. A Thorlabs FL780-10 780 nm filter selected the signal wavelength before a Mako G-319C POE camera. The IR transmittance of un-implanted diamond and the region of lowest doping is similar, 66 - 74 %, and the more highly doped regions transmit less IR light, 14 - 26 %. To account for variation in transmittance across the diamond, we also compared transmittance in each boron-implanted region to the un-implanted diamond directly surrounding it. We found the lowest doping reduced transmission by 6 - 8 %, versus 45 - 63 % for the higher dopings. This suggests the least doped region absorbs only slightly more IR than pure diamond, while the highly doped regions absorb much more IR.

4. Conclusion

Characterization of the boron-implanted and annealed diamond showed moderate healing of the 5×10^{15} ions/cm^2 fluence region, and little healing at higher fluencies. The increase in IR transmittance, recovery of the 1332 cm^{-1} micro-Raman peak, and reduction in surface bulge in white-light topography are all signs of healing in the lowest doped region. The RCI also shows significant healing, although the RCI deviations are still greater than the rocking curve width, which reduces its effectiveness as a Bragg-reflecting optic. Additionally, while the 5×10^{15} ions/cm^2

doped region showed significant healing, its high IR transmittance reduces how effectively it could be heated during Q-switching.

In future work, we must increase uniformity of the RCI within the boron-doped regions while keeping IR absorption high. The structure in the RCI within the boron-doped regions is likely due to our procedure of implanting ions in a rastering pattern. For a more uniform RCI in a boron-implanted sample, future studies could use a large ion beam with a mask, rather than rastering.

To avoid reduction in IR absorption with annealing, one might also consider forgoing annealing, and instead reflecting off the opposite surface of the crystal. We expect the other side of the diamond is less damaged by the boron implantation, as boron ions only pass through one side as they are implanted in the crystal. In order for effective heating on the reflection surface, one could machine a diamond drumhead from the back surface of the crystal such that the boron-implanted regions are 5 μm below the new reflecting surface.

As an alternative to boron implantation, if sufficiently high quality, low-strain, single-crystal CVD diamonds can be grown for Bragg-reflecting optics [8], one could attempt boron doping by depositing a layer of boron during crystal growth.

Future developments in diamond boron doping should produce a uniform RCI, enabling future generations of Q-switching Bragg-reflecting optics.

A. Additional Sample Preparation Details

Fig. A.1 shows the pressure and temperature plots from the 1300 °C and 1450 °C annealings. Our furnace maintained a $<1 \times 10^{-4}$ mbar pressure during the highest temperature annealings.

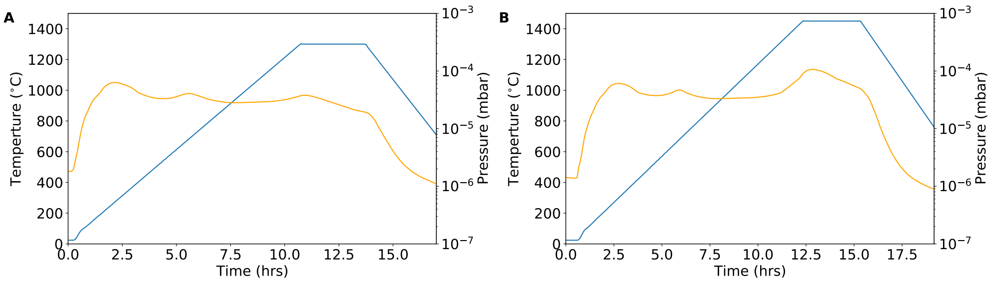

Figure A.1: Example sample annealing temperature and pressure for A) 1300 °C annealing and B) 1450 °C annealing.

B. Additional Images

Fig. B.1 shows 1x magnification images of the diamond at each step in the preparation process. Images have been balanced so that the un-doped regions are of equal brightness. We noticed that the 5×10^{15} ions/cm^2 region lighted following the first 900 °C annealing. We also noticed some graphitization (upper and lower right corners) appeared following the 950 °C annealing in Fig. B.1D-G.

Fig. B.2 shows rocking curve images from the 1150 °C annealing datasets at alternative orientations. These images demonstrate the changes in the recorded RCI from rotating the crystal 90 degrees, and strain on the back side of the approximately 0.4 mm thick crystal.

Fig. B.3 shows the surface height across the crystal from the surface topography measurement. A linear term has been removed from these plots to account for any tilting of the crystal during the measurement.

The authors note that the image data in Fig. B.3B had to be re-constructed from a png with an overlaid colormap after the original file was misplaced. While the features near the boron-doped regions reproduced well, areas at the extremes of the colormaps did not reproduce particularly well. Fig. B.3B likely has more curvature on the left/right sides than is depicted here.

Fig. B.4 shows the accompanying image data for the IR transmittance measurement.

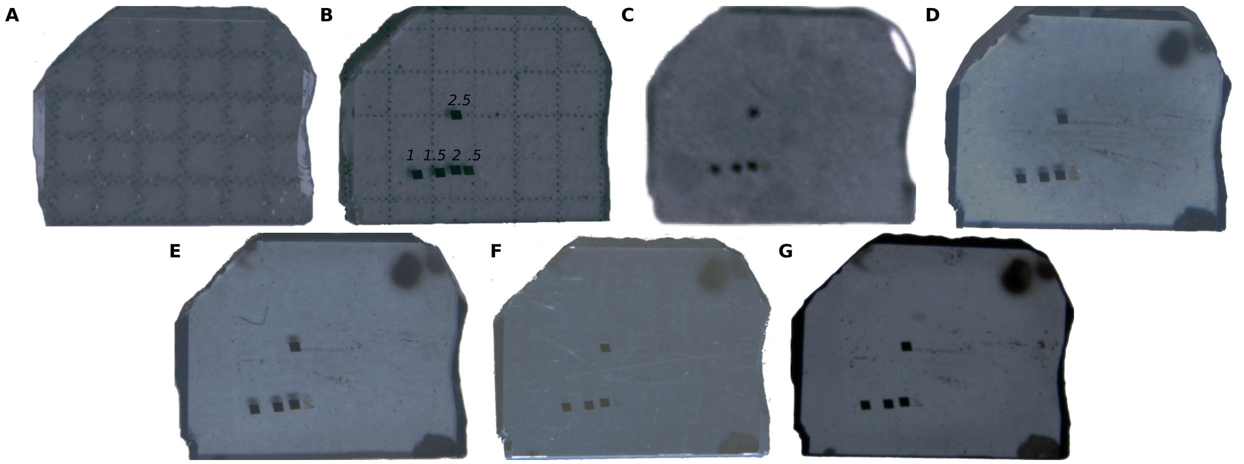

Figure B.1: 1x images for A) pre-implantation, B) pre-annealing, C) post 900 °C annealing, D) post 950 °C annealing, E) post 1150 °C annealing, F) post 1300 °C annealing, G) post 1450 °C annealing. Overlaid numbers give the fluences of the boron implanted regions in units of 1×10^{16} ions/cm^2. A) and B) have been placed on millimeter graph paper to show scale.

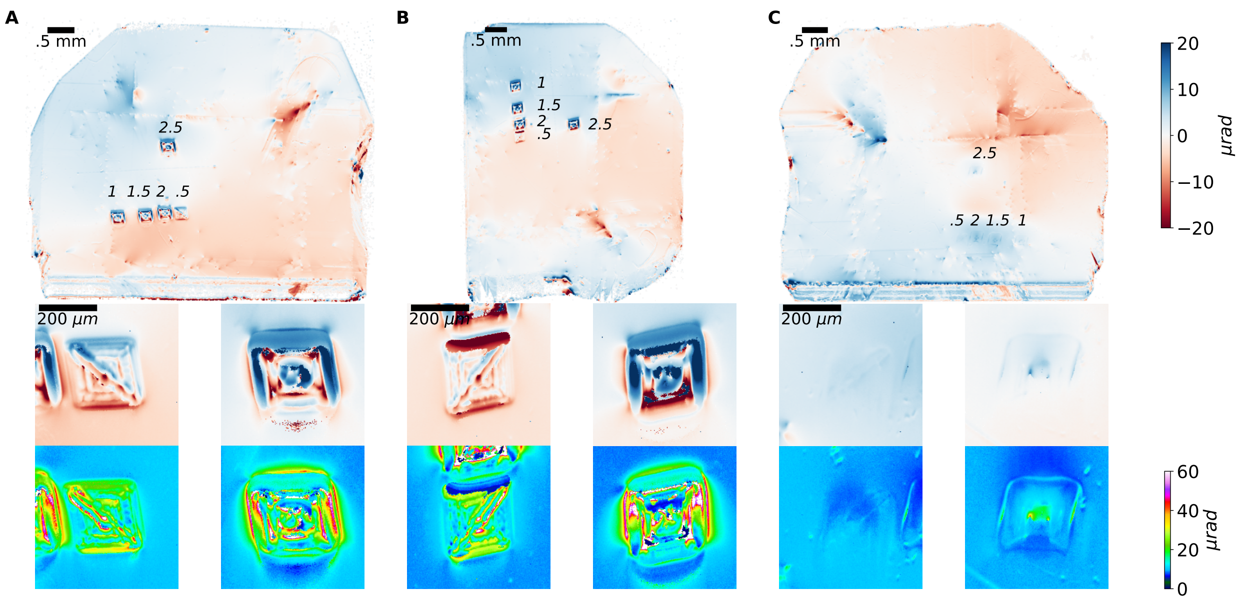

Figure B.2: Rocking-curve images in alternate orientations for the post 1150 °C annealing dataset. A) Nominal orientation, B) 90 ° rotation, C) back side of crystal. Each case shows the rocking-curve center as determined by a Gaussian fit (red-blue colorscale) and the rocking-curve full-width half-maximum (rainbow colorscale). Overlaid numbers give the fluences of the boron implanted regions in units of 1×10^{16} ions/cm^2. The lower images show close-ups of boron-doped regions, 5×10^{15} ions/cm^2 (left) and 2.5×10^{16} ions/cm^2 (right).

CRediT authorship contribution statement

R. A. Margraf: Formal analysis, Methodology, Software, Investigation, Data Curation, Writing - Original Draft, Writing - Review Editing, Visualization. **M. D. Ynsa:** Conceptualization, Methodology, Investigation. **J. Krzywinski:** Conceptualization, Software, Formal Analysis. **A. Halavanau:** Methodology, Investigation, Writing - Original Draft, Writing - Review Editing. **M. L. Ng:** Methodology, Investigation. **J. P. MacArthur:** Methodology, Investigation, Software. **F. Ke:** Methodology, Investigation. **Y. Zhong:** Methodology, Investigation. **S.-K. Mo:** Methodology, Investigation. **P. Pradhan:** Methodology, Investigation. **R. Robles:** Methodology, Investigation. **A.**

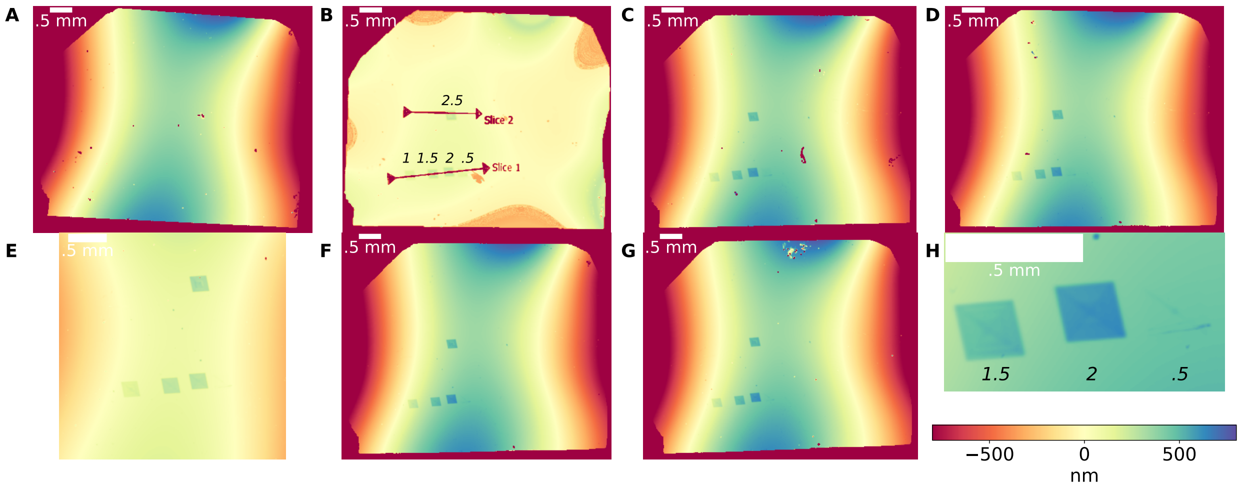

Figure B.3: White light surface topography, showing surface height across the full area of crystal for A) pre-implantation, B) pre-annealing, C) post 900 °C annealing, D) post 950 °C annealing, E) post 1150 °C annealing, F) post 1300 °C annealing, G) post 1450 °C annealing. H) shows a close up of three regions from the post 1450 °C annealing case. Overlaid numbers give the fluences of the boron implanted regions in units of 1×10^{16} ions/cm^2.

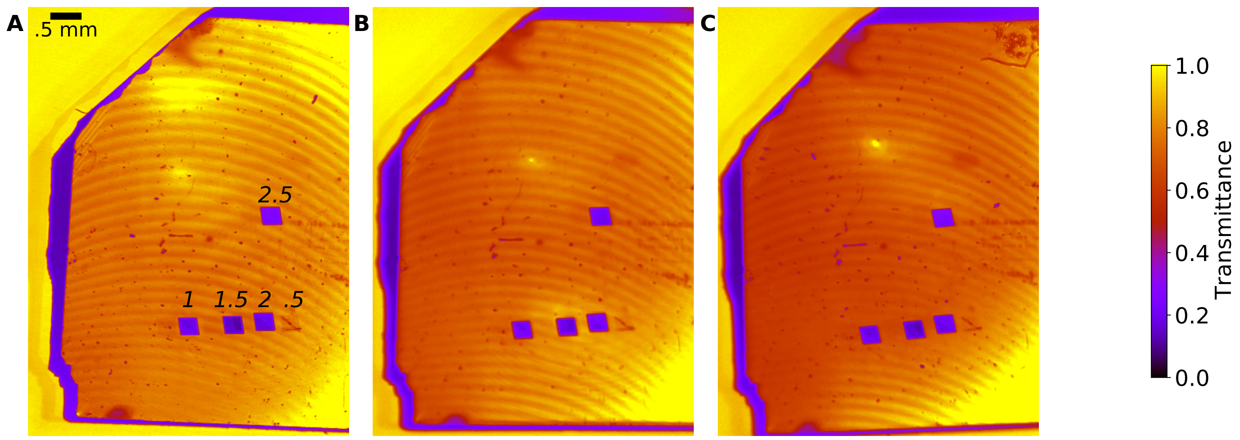

Figure B.4: IR transmittance images, A) post 1150 °C annealing, B) post 1300 °C annealing, C) post 1450 °C annealing. Overlaid numbers give the fluences of the boron implanted regions in units of 1×10^{16} ions/cm^2.

Robert: Methodology, Investigation. **T. Sato:** Methodology, Investigation. **D. Zhu:** Methodology, Investigation, Resources, Project administration. **G. Marcus:** Conceptualization, Resources, Project administration.

Acknowledgements

This work was supported by the Department of Energy, Laboratory Directed Research and Development program at SLAC National Accelerator Laboratory, under contract DE-AC02-76SF00515.

Boron implantation was performed by María Dolores Ynsa using the microbeam line of the Center for Micro Analysis of Materials (CMAM) at the Autonomous University of Madrid. We thank the technical staff of CMAM for operating the tandem ion-beam accelerator.

Diamond annealings at 900 and 950 °C were performed by Sung-Kwan Mo and Yong Zhong at Lawrence Berkeley National Laboratory. Boron annealings at 1150, 1300, and 1450 °C were performed by Rachel Margraf and James MacArthur at SLAC National Accelerator Laboratory.

Rocking Curve Imaging was performed at three different beamlines. The pre-implantation measurement were made at BL29XUL of SPring-8 with the approval of RIKEN SPring-8 Center (Proposal No. 20190013) by James MacArthur, Aymeric Robert, Takahiro Sato, and Diling Zhu with the help of Yoshiki Kohmura, Taito Osaka and Kenji Tamasaku. The pre-annealing, post-implantation measurement was made at the Advanced Photon Source at Argonne National Laboratory by James MacArthur, Diling Zhu, Takahiro Sato, Alex Halavanau and Paresh Pradhan. The post annealing measurements were made at beamline 10-2 of the Stanford Synchrotron Radiation Light Source at SLAC National Accelerator Laboratory by Alex Halavanau, James MacArthur, Rachel Margraf, River Robles, and Gabriel Marcus, with the help of Olga Kraynis, Christopher Takas, Bart Johnson, Ross Arthur and Diling Zhu.

White light profilometry was performed by May Ling Ng at SLAC National Accelerator Laboratory.

Micro-Raman Spectroscopy was performed by Rachel Margraf and Feng Ke at Stanford University.

IR Transmittance Measurements were performed by Rachel Margraf, with the help of Diling Zhu, at SLAC National Accelerator Laboratory.

Jacek Krzywinski determined parameters for boron implantation via simulation and guided characterization efforts. Rachel Margraf compiled the figures and analysis. Rachel Margraf and Alex Halavanau wrote the manuscript. Gabe Marcus coordinated and led this effort with the assistance of Zhirong Huang and Diling Zhu.

Disclosures

The authors declare no conflicts of interest.

References

[1] J. Krzywiński, Y. Feng, A. Halavanau, Z. Huang, A. M. Kiss, J. P. MacArthur, G. Marcus, T. Sato, D. Zhu, Q-Switching of X-Ray Optical Cavities by Using Boron Doped Buried Layer Under a Surface of a Diamond Crystal, in: 39th International Free Electron Laser Conference, 2019, p. TUP033. doi:10.18429/JACoW-FEL2019-TUP033.

[2] C. J. Wort, R. S. Balmer, Diamond as an electronic material, Materials Today 11 (2008) 22–28. URL: https://www.sciencedirect.com/science/article/pii/S1369702107703498. doi:https://doi.org/10.1016/S1369-7021(07)70349-8.

[3] S. A. Stepanov, X-ray server: an online resource for simulations of x-ray diffraction and scattering, Denver, CO, 2004, pp. 16–26. URL: http://proceedings.spiedigitallibrary.org/proceeding.aspx?articleid=849725. doi:10.1117/12.557549.

[4] M. Ynsa, M. Ramos, N. Skukan, V. Torres-Costa, M. Jakšić, Highly-focused boron implantation in diamond and imaging using the nuclear reaction $^{11}\mathbb{B}(\mathbb{p},\alpha)^{8}\mathbb{Be}$ 348 (2015) 174–177. URL: https://linkinghub.elsevier.com/retrieve/pii/S0168583X14009173. doi:10.1016/j.nimb.2014.11.036.

[5] P. Pradhan, M. Wojcik, X. Huang, E. Kasman, L. Assoufid, J. Anton, D. Shu, S. Terentyev, V. Blank, K.-J. Kim, Y. Shvyd'ko, Small Bragg-plane slope errors revealed in synthetic diamond crystals 27 (2020) 1553–1563. URL: https://scripts.iucr.org/cgi-bin/paper?S1600577520012746. doi:10.1107/S1600577520012746.

[6] A. Halavanau, R. Margraf, R. Robles, J. MacArthur, Z. Qu, G. Marcus, J. Wu, T. Sato, D. Zhu, C. J. Takacs, R. Arthur, O. Kraynis, B. Johnson, T. Rabedeau, Experimental setup for high-resolution characterization of crystal optics for coherent X-ray beam applications 56 (2023). URL: https://scripts.iucr.org/cgi-bin/paper?S1600576722010998. doi:10.1107/S1600576722010998.

[7] M. Ynsa, F. Agulló-Rueda, N. Gordillo, A. Maira, D. Moreno-Cerrada, M. Ramos, Study of the effects of focused high-energy boron ion implantation in diamond 404 (2017) 207–210. URL: https://linkinghub.elsevier.com/retrieve/pii/S0168583X17300678. doi:10.1016/j.nimb.2017.01.052.

[8] S. Stoupin, T. Krawczyk, Z. Liu, C. Franck, Selection of CVD Diamond Crystals for X-ray Monochromator Applications Using X-ray Diffraction Imaging 9 (2019) 396. URL: https://www.mdpi.com/2073-4352/9/8/396. doi:10.3390/cryst9080396.